Available online at www.sciencedirect.com
SCIENCE DIRECT®

Journal of the European Ceramic Society 23 (2003) 1269–1276
www.elsevier.com/locate/jeurceramsoc

Microstructure and fracture toughness of a spark plasma sintered Al_2O_3-based composite with $BaTiO_3$ particulates

Sirirat Rattanachan, Yukio Miyashita, Yoshiharu Mutoh*

Department of Mechanical Engineering, Nagaoka University of Technology, 1603-1 Kamitomioka, Nagaoka-shi 940-2188, Japan

Received 30 April 2002; received in revised form 31 July 2002; accepted 7 August 2002

Abstract

Dense Al_2O_3-based composites with dispersed $BaTiO_3$ particulates were fabricated by using spark plasma sintering (SPS) at sintering temperatures between 1100 and 1500 °C with a heating rate of 100 °C/min. High-density of $BaTiO_3$–Al_2O_3 with various compositions could be achieved by SPS at lower sintering temperatures compared to those by conventional pressure-less sintering (PLS). However, full densification was prevented by the onset of abnormal grain growth in Al_2O_3–$BaTiO_3$ composites sintered by SPS. It was found that SPS process could accelerate the abnormal grain growth due to the activation and purification of particle surface. The addition of $BaTiO_3$ in Al_2O_3 matrix improved fracture toughness of the composites fabricated by both SPS and PLS. The highest fracture toughness of 6.04 MPa.m$^{1/2}$ was achieved in the composite sintered by SPS process with 5 mol% $BaTiO_3$, while that of the monolithic Al_2O_3 was about 4.0 MPa.m$^{1/2}$.

Keywords: Al_2O_3; $BaTiO_3$; Composites; Sintering; Toughness and toughening

1. Introduction

Since ceramic materials have various advantages to demonstrate their functions, there are many potential applications. However, ceramics are brittle and show catastrophic fracture. The objective of many researches concerned with structural ceramics is the development of materials with high reliability. The toughening approach attempts to create microstructures that result in sufficient fracture resistance. In addition, intelligent materials with self-sensing function, self-effecting function, etc. have been widely studied.[1]

The ferroelectric material has an interesting mechanical–electrical coupling properties.[2,3] The electric fields can influence the fracture toughness of ferroelectric material. For example, polarized ferroelectrics exhibit anisotropic fracture toughness. The material is tougher for a crack parallel to the poling direction but less tough for a crack perpendicular to it.[2] When an electric field is applied to polarized ferroelectrics, a positive field reduces its fracture toughness but a negative field enhances it. In the past few years, Niihara and his colleagues have proposed ferroelectric-based nanocomposites with high strength and toughness, such as PZT/Pt,[4] $BaTiO_3/MgO$[5] and $BaTiO_3$/SiC.[6] Many researchers have extensively investigated their excellent mechanical properties and also electrical properties such as dielectric constant and the Curie temperature. Since the strain change due to the electro-magnetic field is a physical reaction, piezoelectric-particle-dispersed ceramics would have an advantage that strain sensing function can be directly obtained through measuring the electric field. Chen and his colleagues have proposed a novel approach to toughening of ceramics, where piezoelectric secondary phases were introduced into the matrix such as $BaTiO_3/Al_2O_3$,[7] $BaTiO_3$/3Y-TZP,[8] $Nd_2Ti_2O_7/Al_2O_3$,[9] $Sr_2Nb_2O_7$/3Y-TZP[10] and $BaTiO_3/ZrO_2$,[11] and the energy dissipation due to the piezoelectric effect and domain wall's motion was suggested as the main toughening mechanism.

Spark plasma sintering (SPS) is one of the solid consolidation processes and is carried out in a graphite mold but the heating is accomplished by spark discharges in voids between particles.[12] SPS has the

* Corresponding author. Tel.: +81-258-47-9735; fax: +81-258-47-9770.
E-mail address: mutoh@mech.nagaokaut.ac.jp (Y. Mutoh).

0955-2219/03/$ - see front matter © 2002 Elsevier Science Ltd. All rights reserved.
PII: S0955-2219(02)00294-7

combination of pulsed electrical discharge with rapid heating and pressure application to achieve fast sintering of powders. Takeuchi et al.[13] fabricated dense barium titanate ceramics (97% relative density) with submicrometer-sized grains by SPS, where the grain size is about 0.6 μm and almost the same as that of starting powders. They also produced dense $PbTiO_3$ ceramics with submicrometer-sized grains by the SPS process.[14]

In the present work, ferroelectric $BaTiO_3$ dispersed Al_2O_3 ceramics were sintered by SPS as well as conventional pressure less sintering (PLS). Toughening effect of the composite was investigated together with the microstructural characterization.

2. Experimental procedure

2.1. Materials and sintering procedure

Commercial $BaTiO_3$ powders (BT-05, Sakai chemical industrial Co. Ltd.) with an average particle size of 0.5 μm and high purity Al_2O_3 powders (Sumitomo Sekitan Kougyo, KK) with an average particle size of 0.2 μm were used as the starting materials. Compositions of these powders are shown in Table 1.

The x $BaTiO_3/(1-x)Al_2O_3$ composite powders ($x=0.01$, 0.03, 0.05 and 0.10) were mixed by a ball milling machine with alumina balls in ethanol for 24 h. The wet slurry was then dried by using a rotary evaporator. Dried powders were milled again and sieved through a 150-μm mesh screen. The mixed granules were put into a graphite die with diameter of 25 mm which was on the vibration table for homogeneous packing of the powders and then were sintered using a spark plasma sintering machine by heating at sintering temperatures between 1100 and 1500 °C under a pressure of 38 MPa at a heating rate of 100 °C/min in vacuum. The soaking time at the sintering temperature was 3–5 min and cooling time from the sintering temperature to 600 °C was about 30 min. The temperature was measured by means of an optical pyrometer focused on the graphite die surface.

A conventional PLS of the composite powders was also conducted for comparison. The mixed granules with PVA binder were formed into rectangular bars by uniaxially pressing and then compacted by cold isostatic pressing (CIP) at 200 MPa. The compacts were fired in a furnace at temperatures ranged from 1300 to 1450 °C for 2 h in air at a heating rate of 10 °C/min. Dimensions of the bar were 15 mm in width, 15 mm in height and 80 mm in length. The monolithic alumina was also prepared by the same sintering methods.

2.2. Characterization

The bulk density was determined by Archimedes' method in water. The X-ray diffraction (XRD) analysis was conducted using Shimadzu XRD 6100 with nickel-filtered Cu K_α radiation. The average grain size and pore size of the samples were determined from scanning electron micrographs on the polished and etched surfaces.

2.3. Fracture toughness testing

Fracture toughness was evaluated by the indentation fracture (IF) method with the equation proposed by Niihara et al.[15] Indentation racks were induced at a load of 98 N for 15 s using a Vickers hardness tester. The indentation crack path was observed by using a scanning electron microscope (SEM) in detail.

3. Results and discussion

3.1. XRD analysis

From the results of XRD analysis, some intermediate phases such as $BaAl_{13.2}O_{20.8}$ and $BaAl_6TiO_{12}$ as well as $BaTiO_3$ and Al_2O_3 phases were found, as shown in Fig. 1. Relative X-ray peak intensities of these phases are listed in Table 2. Because of reaction between $BaTiO_3$ and Al_2O_3, the $BaTiO_3$ secondary phase was significantly reduced. The peak angles of $BaTiO_3$ and $BaAl_{13.2}O_{20.8}$ are almost identical. It is then difficult to distinguish the two phases. In the figure, the intensity of $BaAl_{13.2}O_{20.8}$ includes that of $BaTiO_3$. The total amount of the intermediate phases increased with increasing the amount of $BaTiO_3$ addition and sintering temperature.

Table 1
Characterization of barium titanate powder (BT-05) and alumina powder

	α- Al_2O_3	Si	Fe	Na	K	Ca	Mg	BET analysis (m^2/g)	Ave. particle size (μm)
Al_2O_3 powder	99.99%	6 ppm	7 ppm	3 ppm	1 ppm	1 ppm	1 ppm	12.9	0.20
	Ba/Ti ratio	SrO (wt%)	CaO	Na_2O	SiO_2	Al_2O_3	Fe_2O_3		
$BaTiO_3$ powder	1.00	0.01	<0.001	0.001	0.001	<0.001	0.001	2.4	0.5

3.2. Microstructure

Figs. 2 and 3 show microstructures of monolithic alumina and $BaTiO_3$–Al_2O_3 composites sintered at 1200 and 1300 °C by SPS, respectively. Al_2O_3, intermediate and $BaTiO_3$ grains in the SEM micrographs (Back scattering electrons image) are black, gray and white regions, respectively. From Fig. 2, it is seen that the samples with 3 and 5 mol% $BaTiO_3$ were not well sintered at 1200?, where isolated powders were observed, while the sample with 10 mol% $BaTiO_3$ was well sintered. It is seen from Fig. 3 that the samples were well sintered at 1300 °C. For the sintering temperatures lower than 1200° and higher than 1300 °C, the samples were crashed and/or cracked during the sintering process. It is also found that the $BaTiO_3$ phase was not uniformly distributed in the Al_2O_3 matrix phase. Fig. 4 shows microstructures of monolithic alumina and $BaTiO_3$-Al_2O_3 composites sintered by PLS. It can be seen from the figure that there are lots of small pores. For the sintering temperatures lower than 1400 °C, it seemed that dense samples could not be obtained.

Average grain size of monolithic alumina sintered by SPS was approximately 1–2 μm with larger grain sizes up to 4 μm, while that by PLS was about 8 μm. Smaller grain size can be obtained by SPS compared to conventional

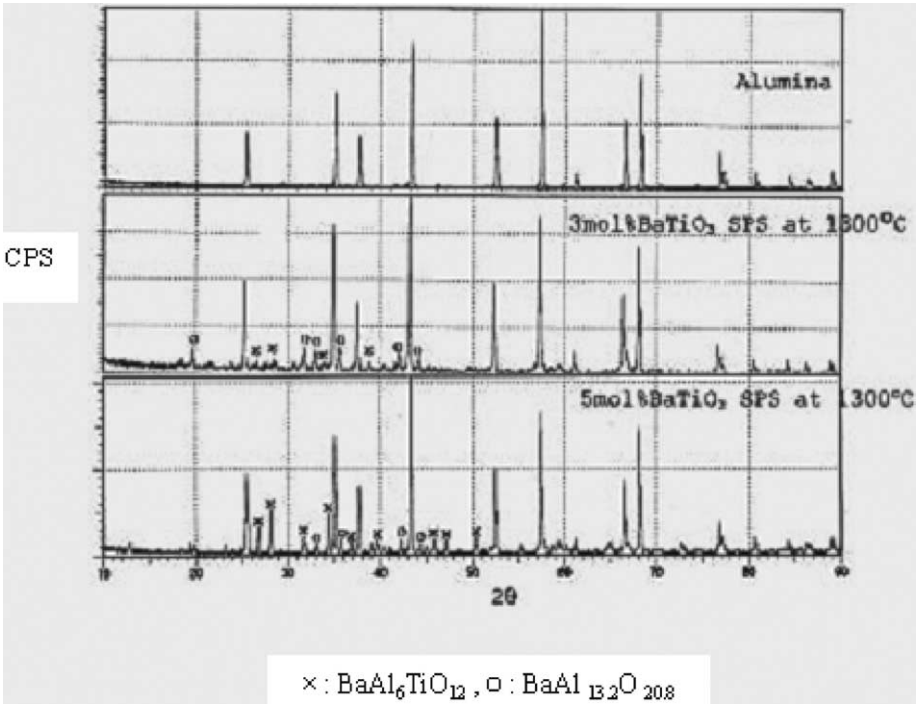

Fig. 1. X-ray diffraction patterns of x $BaTiO_3/(1-x)$ Al_2O_3 composites with $x=0$, 0.03 and 0.05 sintered by SPS at 1300 °C.

Table 2
Characterization of sintered composites

Sintering method	Sintering temp. (°C)	%mol $BaTiO_3$	Relative X-ray peak intensity of phases analysis			Average alumina matrix grain size (μm)
			$I_{BATO}/I_{Al_2O_3}$	$I_{BAO}/I_{Al_2O_3}$	Total of $I_{BATO}+I_{BAO}$	
PLS	1400	3	0.051	0.045	0.096	5.84
		5	0.186	0.063	0.249	3.8
	1450	3	0.139	0.050	0.189	6.6
		5	0.288	0.081	0.369	4.2
SPS	1200	3	0.034	0.049	0.083	0.50
		5	0.076	0.063	0.139	0.53
	1300	3	0.038	0.108	0.146	0.6/6.406
		5	0.118	0.086	0.204	0.625/6.80

Abbreviation: BATO:$BaAl_6TiO_{12}$, BAO:$BaAl_{13.2}O_{20.8}$.

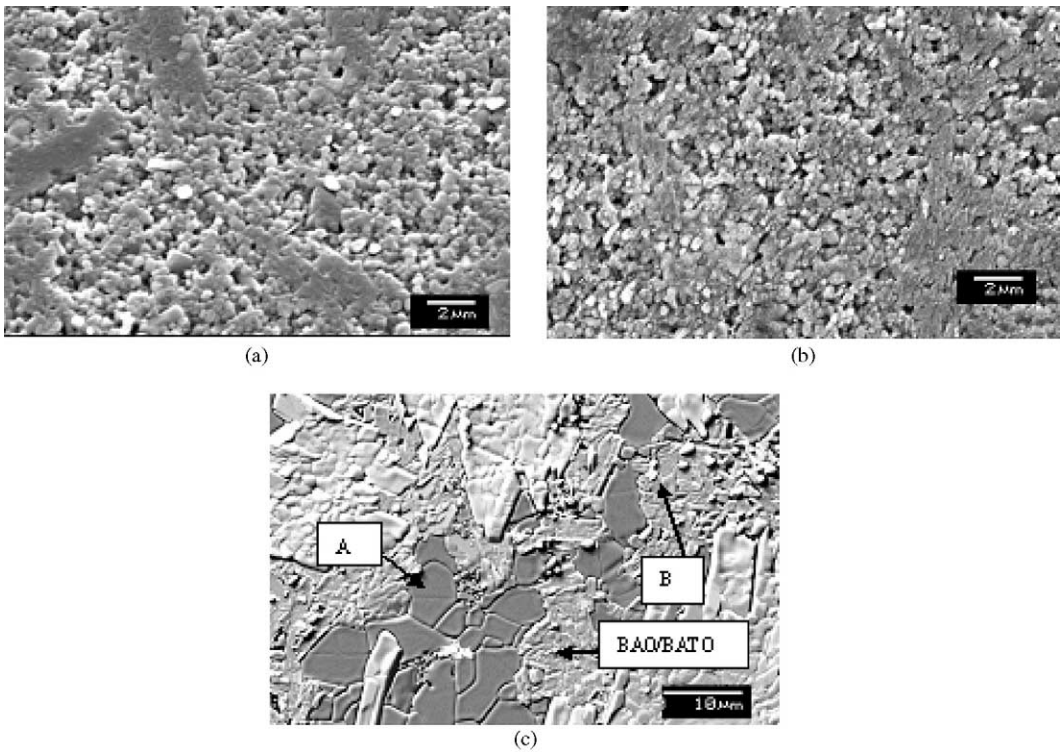

Fig. 2. Scanning electron micrographs of thermal etched surface of $x\mathrm{BaTiO_3}/(1-x)\mathrm{Al_2O_3}$ composites sintered by SPS (a) $x=0.03$, (b) $x=0.05$ and (c) $x=0.10$ at 1200 °C. A: Al_2O_3 phase, B: $BaTiO_3$ phase and BAO/BATO: intermediate phase.

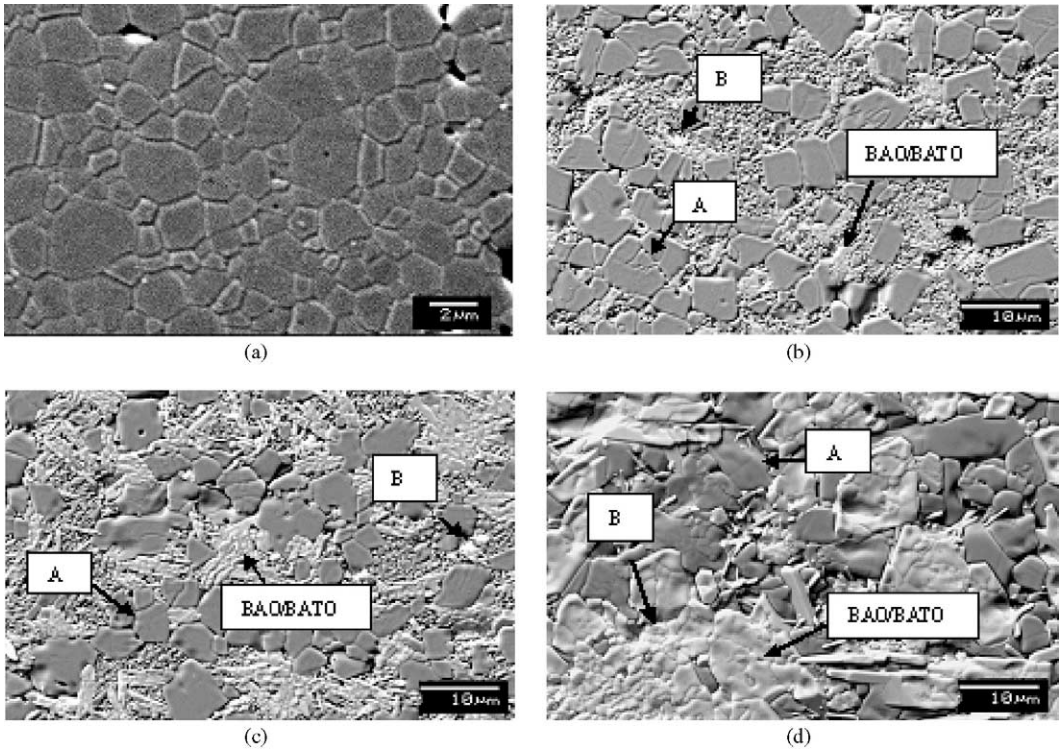

Fig. 3. Scanning electron micrographs of thermal etched surface of $x\mathrm{BaTiO_3}/(1-x)$ $\mathrm{Al_2O_3}$ composites sintered by SPS (a) $x=0$, (b) $x=0.01$, (c) $x=0.03$, (d) $x=0.05$ at 1300 °C. A: Al_2O_3 phase, B: $BaTiO_3$ phase and BAO/BATO: intermediate phase.

PLS. Average alumina grain sizes of $BaTiO_3$–Al_2O_3 composites are listed in Table 2. The average alumina grain sizes of the composites sintered by SPS were significantly small compared to those by PLS by a factor of 10. The grain sizes increased with increasing sintering temperature.

The microstructures of composites with 3 and 5 mol% $BaTiO_3$ sintered by SPS at 1300 °C were bimodal with large grains in fine-grain matrix, as shown in Fig. 3(b), (c) and (d). The size of large grain of the SPS composites increased dramatically with increasing $BaTiO_3$ content. The large grains grew longitudinally to plate-like shape. Large plate-like grains, which have grown at the expense of small ones, may represent coarsening under the presence of liquid phase. From BaO–TiO_2 system,[16] $BaTiO_3$ can form liquid phase at 1322 °C. This result suggests that small amount of $BaTiO_3$ addition to Al_2O_3 leads to liquid phase being formed at the grain boundaries, which enhances surface diffusion and hence grain growth.

From Fig. 3, large pores were observed at grain boundaries and the grain size was almost the same regardless of $BaTiO_3$ content. Fig. 3 also shows the agglomerated $BaTiO_3$ grains and suggests the aggregated of intermediate phase being formed at grain boundaries. Thus, the addition of $BaTiO_3$ is deleterious for the fabrication of dense $BaTiO_3$–Al_2O_3 composites with fine grains.

3.3. Density

Relationships between relative density and sintering temperature for $BaTiO_3$–Al_2O_3 composites sintered by SPS and PLS are shown in Fig. 5. It can be seen from

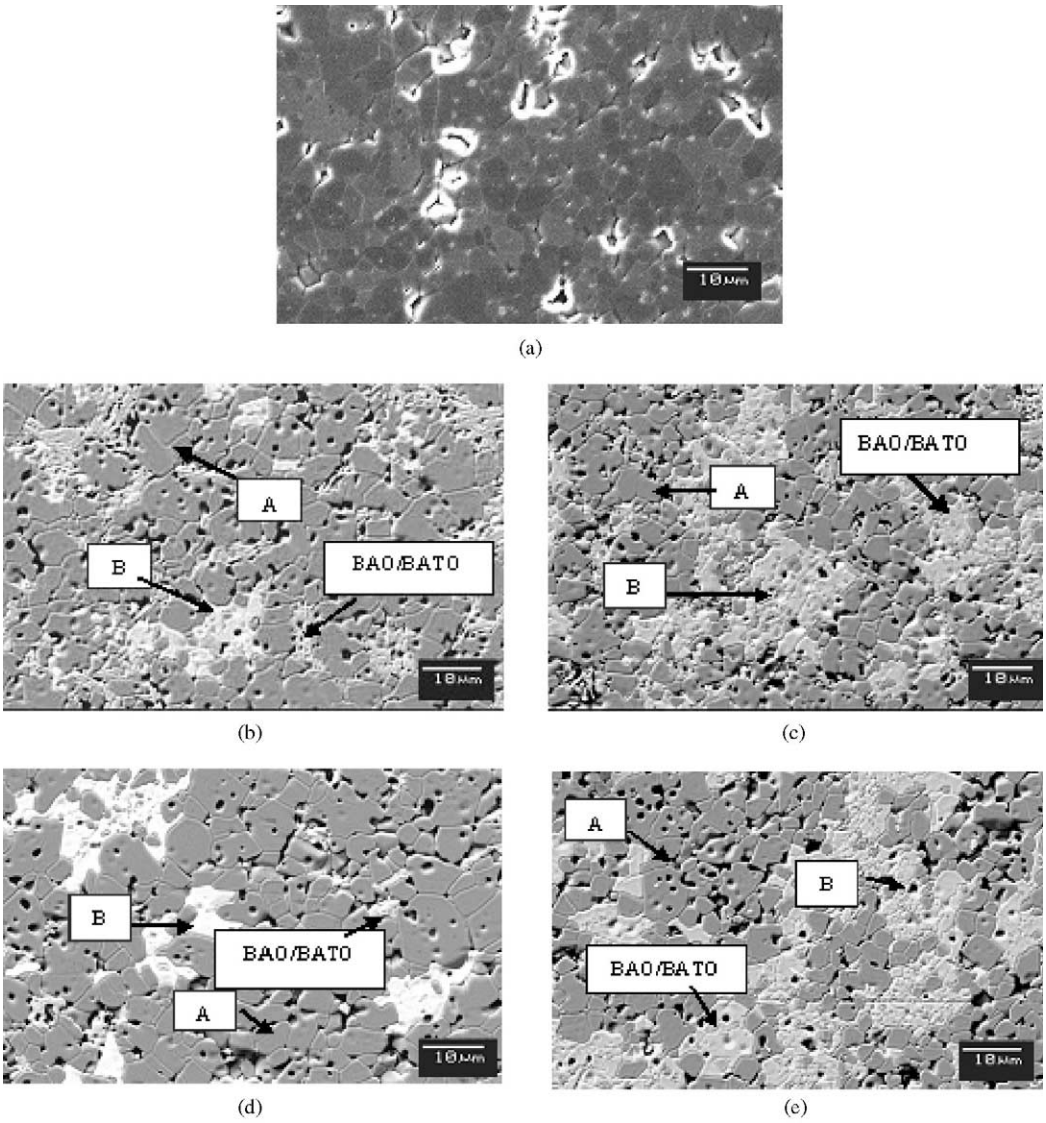

Fig. 4. Scanning electron micrographs of thermal etched surface of $x BaTiO_3/(1-x)Al_2O_3$ composites sintered by PLS (a) $x=0$, (b) $x=0.03$, (c) $x=0.05$ at 1400 °C and (d) $x=0.03$, (e) $x=0.05$ at 1450 °C. A: Al_2O_3 phase, B: $BaTiO_3$ phase and BAO/BATO: intermediate phase.

the figure that the relative density increased with increasing sintering temperature. Higher relative density of the composites could be obtained by SPS compared to PLS. Fig. 6 shows relationship between density of $BaTiO_3$–Al_2O_3 composites and $BaTiO_3$ content. As can be seen from the figure, density decreased with increasing $BaTiO_3$ content for both SPS and PLS methods. The highest densification of SPS samples was attained in the $BaTiO_3$–Al_2O_3 composite sintered at 1300 °C, while it was not successful to densify at sintering temperatures above 1300 °C. Since the temperature inside the graphite die is higher than the temperature measured on the surface of die by about 100–200 °C, process-induced flaws might be caused by the hexagonal-cubic transition of $BaTiO_3$ (at 1460 °C) associated with the high cooling rate of SPS system. Furthermore, the composites with addition of $BaTiO_3$ indicated lower density than monolithic Al_2O_3.

3.4. Hardness

Fig. 7 shows relationship between Vickers hardness and $BaTiO_3$ content for the composites sintered by SPS and PLS. The hardness decreased with increasing $BaTiO_3$ content and sintering temperature. SPS produced higher hardness materials compared to PLS. This may caused by the finer grains as well as higher density of SPS composites.[17]

3.5. Fracture toughness

Fig. 8 shows relationship between fracture toughness K_{IC} and $BaTiO_3$ content. The scatter bands of the data are also indicated in the figure, while they are rather large. From the figure, fracture toughness of the $BaTiO_3$–Al_2O_3 composite sintered at 1300 °C by SPS was significantly improved with increasing the amount of $BaTiO_3$ addition up to 5 mol%. The maximum fracture toughness of 6.04 MPa.m$^{1/2}$ was obtained for the composition of –5 $BaTiO_3$ 95Al_2O_3, while the fracture

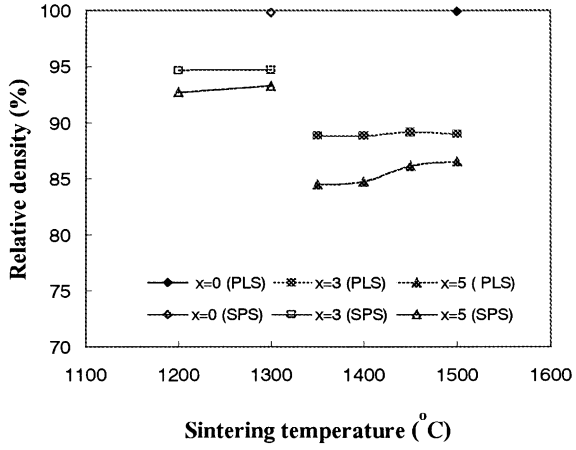

Fig. 5. Relationship between sintering temperature and relative density of xBaTiO$_3$/(1−x) Al_2O_3 composite sintered by SPS and PLS.

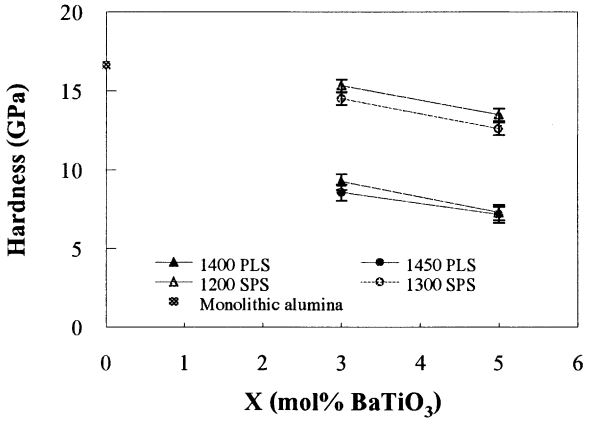

Fig. 7. Vickers hardness vs. $BaTiO_3$ content for $BaTiO_3$–Al_2O_3 composites sintered by SPS and PLS.

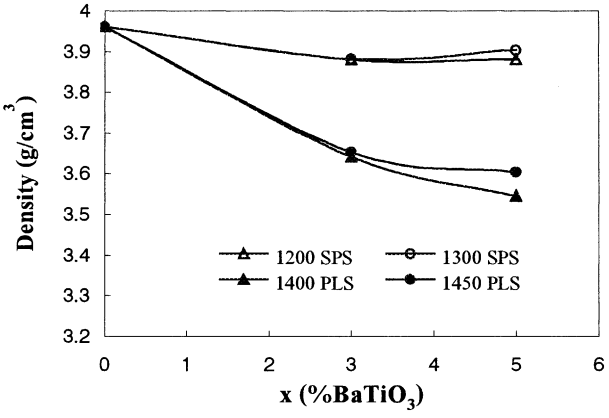

Fig. 6. Relationship between density of xBaTiO$_3$/(1−x) Al_2O_3 composite and $BaTiO_3$ content.

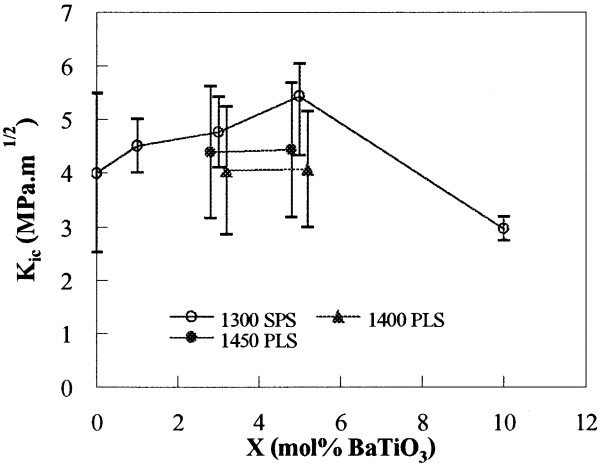

Fig. 8. Fracture toughness vs. $BaTiO_3$ content for $BaTiO_3$–Al_2O_3 composites sintered by SPS and PLS.

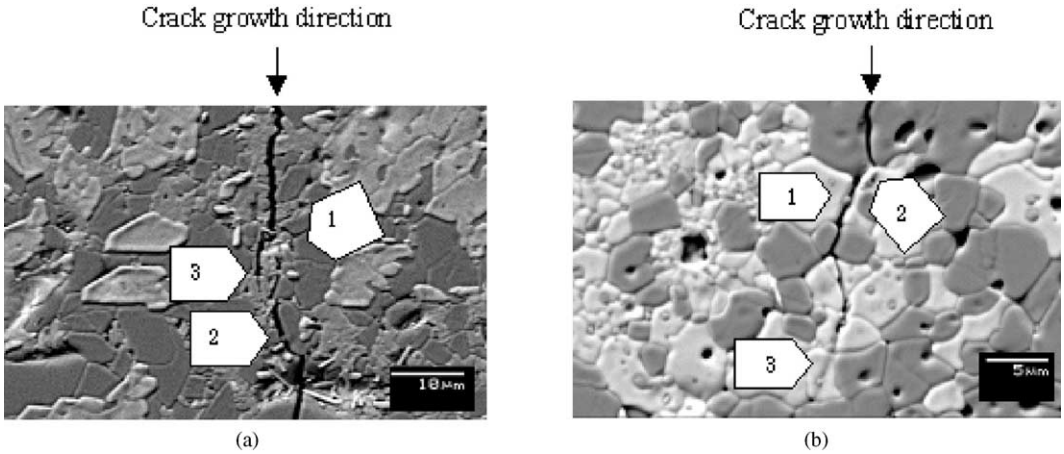

Fig. 9. Indentation cracks on polished surface of (a) 5 mol% $BaTiO_3$–SPS composite at 1300 °C and (b) 3 mol%$BaTiO_3$–PLS composite at 1450 °C. The white arrows are indicated as: 1 = deflection at or near $BaTiO_3$ particles, 2 = crack bridging, 3 = crack arresting at or in the intermediate phases.

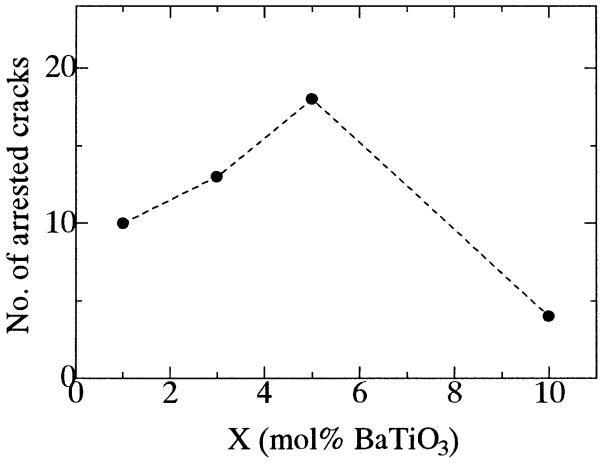

Fig. 10. The numbers of arrested indentation cracks at intermediate phases as function of $BaTiO_3$ content.

toughness of monolithic Al_2O_3 was about 4 MPa.$m^{1/2}$. When the content of $BaTiO_3$ increased up to 10 mol%, fracture toughness of the composite sintered at 1300 °C by SPS was significantly reduced. Fracture toughnesses of the $BaTiO_3$–Al_2O_3 composites sintered by PLS were equal to or higher than that of monolithic Al_2O_3.

Fig. 9 shows examples of the crack paths for the fracture toughness test specimens. It can be seen from the figure that there are three typical features of the crack path: (1) crack deflection at or near $BaTiO_3$ particles, (2) crack bridging, and (3) crack arresting at or in the intermediate phases. The crack bridging and arresting at or in the intermediate phases were often observed on the crack wake, as shown in the figure. Fig. 10 shows the number of arrested cracks at or in the intermediate phase as a function of amount of $BaTiO_3$ addition for the samples sintered by SPS at 1300 °C. In the figure, the total number of observed cracks was 24 for each sample. It can be seen from the figure that the number of arrested cracks increased with increasing the $BaTiO_3$ content up to the amount of 5 mol% and then decreased. This tendency agrees well with that of fracture toughness shown in Fig. 8, which suggests higher toughness of the intermediate phases compared to that of Al_2O_3 matrix. It is well known that crack bridging significantly reduces the crack tip stresses and then enhances the crack growth resistance.[18] Therefore, the intermediate phases will significantly contribute the higher fracture toughness. The crack deflection at or near $BaTiO_3$ particles was also observed. It is also known that ferroelectric phases will induce compressive stress around them during loading process due to stress-induced domain switching and then contribute the improvement of fracture toughness.[7,19–22] In an unpolarized piezoelectric domain switching is also possible if those domains are in a suitable orientation. However, since the $BaTiO_3$ phase easily reacted with the Al_2O_3 phase and the intermediate phases were produced, the only small amount of $BaTiO_3$ phase remained in the samples. Therefore, the effect of $BaTiO_3$ phase on fracture toughness of the present samples may not be dominant, while the phase will have some effect on toughness in its nature.

4. Conclusion

Piezoelectric secondary phase dispersed ceramic composites, $BaTiO_3$–Al_2O_3, could be produced by the SPS method and densed composites could be obtained in contrast to that by the PLS method. The highest densification of SPS samples (95% relative theoretical density) was attained in $BaTiO_3$–Al_2O_3 ceramics at the sintering temperature of 1300 °C by SPS, while the densification was not successful at sintering temperatures above 1300 °C. The relative density of sintered SPS

composites was higher than that of sintered PLS composites. The relative density of $BaTiO_3$–Al_2O_3 composites was decreased with increasing $BaTiO_3$ content. The microsturcture of sintered SPS composites indicated fine alumina grains with some abnormal grain growth of intermediate phases. The abnormal grain growth could be caused by the spark discharge happened between the particles, which increased the surface activity of the powder and then accelerated the surface diffusion. However, the fracture toughness of the $BaTiO_3$–Al_2O_3 composites was improved and the highest fracture toughness of 6.04 MPa.$m^{1/2}$ for the Al_2O_3 with 5 mol% $BaTiO_3$ sintered by SPS at 1300 °C was achieved.

Crack bridging and crack arresting at or in the intermediate phases were increasingly observed in the higher toughness samples, which indicates that the intermediate phases must contribute to the higher fracture toughness. The crack deflection at or near $BaTiO_3$ particles was also observed. However, only small amount of $BaTiO_3$ phase remained in the present composites and then the contribution to higher fracture toughness will be not significant. If large amount of $BaTiO_3$ phase could be remained in the composite, fracture toughness will be improved further, which will be the next work.

Acknowledgements

The authors would like to thank Macoho Co., Ltd. for helping to use SPS machine and Uematsu laboratory, department of chemistry, Nagaoka University of Technology for cold isostatic pressing machine.

References

1. Kishimoto, A., Ishida, H. and Nakamura, Y., Design and fabrication of a strength controllable ceramic composite. *J. Ceram. Soc. Japan*, 1998, **106**, 537–538.
2. Wang, H. and Singh, R. N., Crack propagation in piezoelectric ceramics under pure mechanical loading. *Ferroelectrics*, 1998, **207**, 555–575.
3. Hwang, S. C., Lynch, C. S. and McMeeking, R. M., Ferroelectric/ferroelastic interactions and a polarization switching model. *Acta Metall. Mater.*, 1995, **43**, 2073–2084.
4. Hwang, H. J., Tajima, K.-I., Sando, M., Toriyama, M. and Niihara, K., Microstructure and mechanical properties of lead zirconate titanate (PZT) nanocomposites with platinum particles. *J. Ceram. Soc. Japan*, 2000, **108**, 339–344.
5. Hwang, H. J., Nagai, T., Sando, M., Toriyama, M. and Niihara, K., Fabrication of piezoelectric particle-dispersed ceramic nanocomposite. *J. Eur. Ceram. Soc.*, 1999, **19**, 993–997.
6. Hwang, H. J., Sekino, T., Ota, K. and Niihara, K., Perovskite-type $BaTiO_3$ ceramics containing particulate SiC. *J. Mat. Sci.*, 1996, **31**, 4617–4624.
7. Chen, X. M. and Yang, B., A new approach for toughening of ceramics. *Mat. Lett.*, 1997, **33**, 237–240.
8. Yang, B., Chen, X. M. and Liu, X. Q., Effect of $BaTiO_3$ addition on structures and mechanical properties of 3Y-TZP ceramics. *J. Eur. Ceram. Soc.*, 2000, **20**, 1153–1158.
9. Yang, B. and Chen, X. M., Alumina ceramics toughened by a piezoelectric secondary phase. *J. Eur. Ceram. Soc.*, 2000, **20**, 1687–1690.
10. Chen, X. M., Liu, X. Q., Liu, F. and Zhang, X. B., 3Y-TZP ceramics toughened by $Sr_2Nb_2O_7$ secondary phase. *J. Eur. Ceram. Soc.*, 2001, **21**, 477–481.
11. Seo, S. and Kishimoto, A., Effect of polarization treatment on bending strength of barium titanate/zirconia composite. *J. Eur. Ceram. Soc.*, 2000, **20**, 2427–2431.
12. Omori, M., Sintering, consolidation, reaction and crystal growth by the spark plasma sintering (SPS). *Mater. Sci. Eng.*, 2000, **A287**, 183–188.
13. Takeuchi, T., Betourne, E., Tabuchi, M. and Kageyama, H., Dielectric properties of spark-plasma-sintered $BaTiO_3$. *J. Mat. Sci.*, 1999, **34**, 917–924.
14. Takeuchi, T. and Tabuchi, M. *et al.*, Synthesis of dense lead titanate ceramics with submicrometer grains by spark plasma sintering. *J. Am. Ceram. Soc.*, 2000, **83**, 541–544.
15. Niihara, K., Morena, R. and Hasselman, D. P. H., Evaluation of K_{ic} of brittle solids by the indentation method with low crack-to-indent ratios. *J. Mater. Sci Lett.*, 1982, **1**, 13–16.
16. Rase, D. E. and Roy, R., Eighth Quarterly Progress Report, 1 April to 30 June, Appendix II. 1953, pp. 32.
17. Rice, R. W., Wu, C. C. and Borchelt, F., Hardness-grain-size relations in ceramics. *J. Am. Ceram. Soc.*, 1994, **77**, 2539–2553.
18. Becher, P. F., Microstructural design of toughened ceramics. *J. Am. Ceram. Soc.*, 1991, **74**, 255–269.
19. Liu, Y. G., Jia, D. C. and Zhou, Y., Microstructure and mechanical properties of a lithium tantalate-dispersed-alumina ceramic composite. *Ceramics International*, 2002, **28**, 111–114.
20. Lu, W., Fang, D.-N., Li, C. Q. and Hwang, K.-C., Nonlinear electric-mechanical behavior and micromechanics modelling of ferroelectric domain evolution. *Acta Mater*, 1999, **47**, 2913–2926.
21. Yang, W. and Zhu, T., Switch-toughening of ferroelectrics subjected to electric fields. *J. Mech. Phys. Solids*, 1998, **46**, 291–311.
22. Mao, S. X., Li, X. and Han, X., Toughening of ferroelectric ceramics under polarization switching. *Mater. Sci. Eng.*, 2000, **A292**, 66–73.